Hindawi
Geofluids
Volume 2020, Article ID 8885633, 15 pages
https://doi.org/10.1155/2020/8885633

Research Article

Quantitative Evaluation for the Threat Degree of a Thermal Reservoir to Deep Coal Mining

Yun Chen[1], **Xinyi Wang**[1,2,3], **Yanqi Zhao**[1], **Haolin Shi**[1], **Xiaoman Liu**[1], **and Zhigang Niu**[4]

[1]*School of Resource and Environment, Henan Polytechnic University, Jiaozuo 454000, China*
[2]*Collaborative Innovation Center of Coalbed Methane and Shale Gas for Central Plains Economic Region of Henan Province, Jiaozuo 454000, China*
[3]*State Collaborative Innovation Center of Coal Work Safety and Clean-Efficiency Utilization, Jiaozuo 454000, China*
[4]*Henan Provincial Coal Geological Survey and Research Institute, Zhengzhou 450052, China*

Correspondence should be addressed to Xinyi Wang; chenyun101205@outlook.com and Yanqi Zhao; zhaoyq@hpu.edu.cn

Received 25 May 2020; Revised 7 September 2020; Accepted 19 October 2020; Published 9 November 2020

Academic Editor: Hualei Zhang

Taking the Suiqi coalfield located in North China as the object, where the coal seam burial depth is more than 1100 m, the water abundance of the roof pore thermal storage aquifer is better than average, the ground temperature is abnormally high, and hydrogeological data are relatively lacking, this paper selects and determines eight index factors that influence the mining of the coalfield. Based on the analytic hierarchy process (AHP), the index factor weight is defined, and then, the threat degree of the roof thermal storage aquifer to the coal mining is quantitatively evaluated and divided by using the fuzzy variable set theory. The evaluation results show that the threat degree of the roof in the eastern region is generally greater than that in the western region and that the closer it is to the coal seam outcrop line, the higher the threat degree is; near the boreholes, in the areas Qs1,Qs5, Qs8, Sx1, Tk5, Zc4, and Zc7, which are close to the hidden outcrop line of the coal seam, the classification characteristic value of the threat degree is greater than 3.5, which is in the high-threat zone for disasters caused by roof thermal storage aquifers during coal seam mining. The area above the medium-threat zone accounts for 71.82% of the total study area, indicating that deep coal mining is affected by multiple factors and that roof water and heat disasters are more likely to occur.

1. Introduction

In North China coalfields and southern Ordos Basin coalfields, minable coal seams are directly or indirectly covered by thermal storage aquifers of different thicknesses and coal seam mining operations face the serious threats of double roof water inrush and geothermal disasters. For example, the normal water inflow of a coal mine in the southern margin of the Ordos Basin reaches 106,520 m^3/d and the water temperature at a depth of 700 m reaches 41°C, which greatly affect the normal production of the coal mine. To ensure the safety of underground mining engineering, the threat degree of the roof thermal storage aquifer has become an urgent problem that needs to be solved in coal mine production through scientific evaluation.

Many scholars have carried out a series of research works on the problem of coal seam roof disasters. The theories and methods formed mainly include the "upper three zones" theory [1–3], the "key layer" theory [4], the "three maps-double prediction method" [5], the mathematical comprehensive evaluation method [6], and the numerical simulation method [7]. Among them, the "upper three zones" theory is the most widely used, and the corresponding empirical formula calculation guides the prediction, evaluation, and prevention of a coal seam roof water inrush [8, 9]. In recent years, some scholars have used comprehensive methods to solve practical production problems. For example, Booth and Breuer and Wu et al. applied MODFLOW software to simulate the hydrological effects of shallow aquifers under the influence of long-wall mining, put forward the change rule of

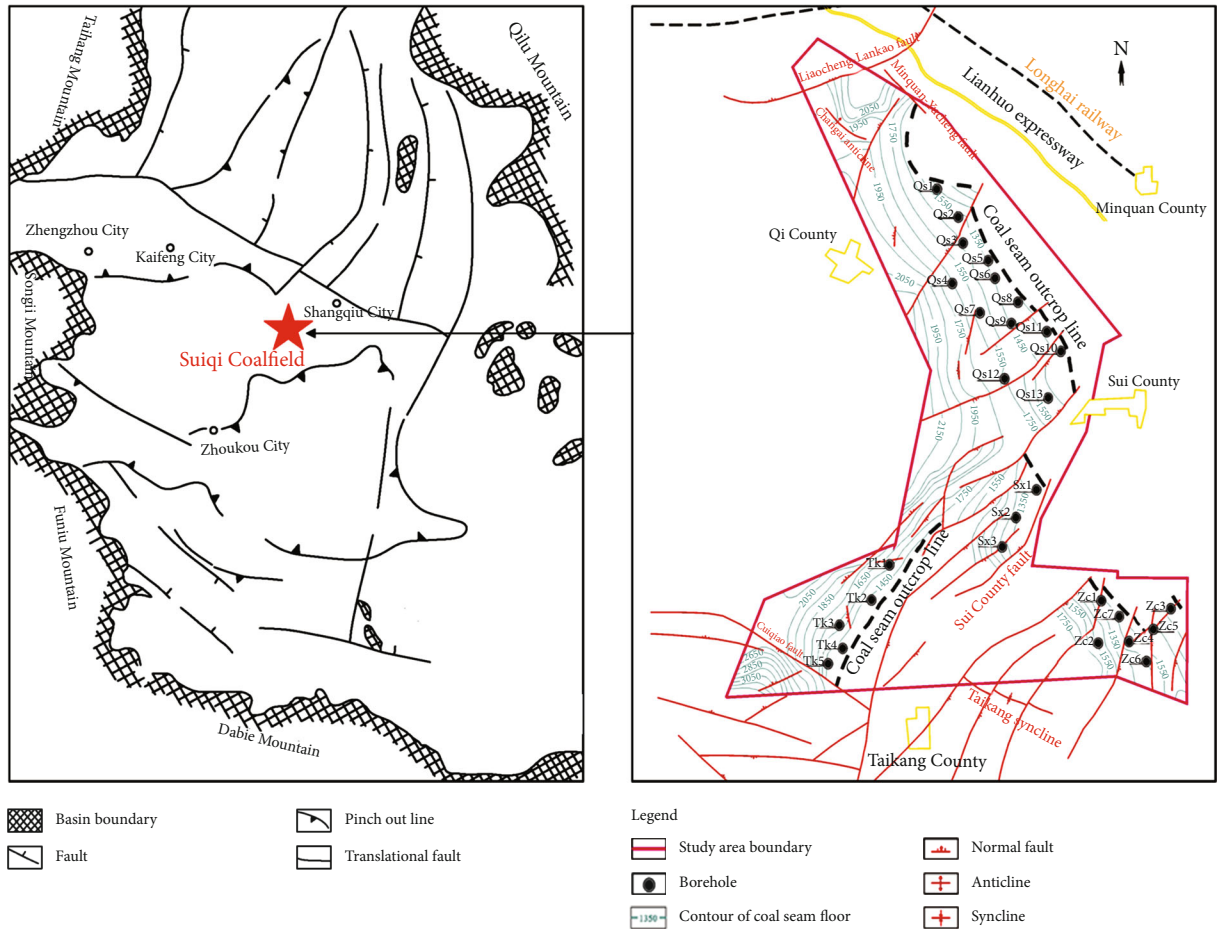

Figure 1: Schematic diagram of the location and geological structure of the Suiqi coalfield.

hydrological parameters, such as the water head with the mining time and space, and hypothesized that the cracks produced during mining caused the water head drop of the aquifer system [10, 11]. Zhou et al. established a conceptual model of mine water inrush composed of a core network, an underground monitoring network, and an operating system, and the underground excavation and water inrush disaster process can be simulated by using the raw underground data [12]. Zhang et al. obtained the height of the "upper three zones" by numerical simulation and used it to study the roof overburden failure [13]. Yang and Sun determined the height of the water flowing through the fractured zone by using a field measurement, numerical simulation, and empirical formulas in the "upper three zones" theory to reasonably determine the size of a waterproof safety coal pillar [14]. Yao et al. used numerical simulation software to simulate the distribution characteristics of the water flowing fracture zone and the seepage characteristics of the roof water during the mining of the workface; additionally, the water inrush risk of the roof aquifer was analyzed [15]. Based on the gray correlation analytic hierarchy process, Zhang and Yang proposed a prediction model for the roof water inrush when mining a shallow coal seam, and the model was verified with engineering examples [16]. Wu et al. and Zeng et al. studied the height of the water flowing fracture zone of the coal seam roof and the richness of the water-rich aquifer and then evaluated the water inrush risk of the aquifer according to the water-rich partition map [17, 18]. Ren and Wu revised the "three figure double prediction method" and evaluated the risk of water inrush in the area where the height of the caving zone formed by coal mining is lower than the elevation of the roof aquifer [19]. Rezaei and Guo et al. used a neural network intelligent prediction model to determine the height of the water flowing fracture zone and evaluate the performance of the model by using a variety of performance indicators (correlation coefficients, variances, etc.) [20, 21]. Ruan et al. proposed a prediction model for the water inrush based on the AHP and the Dempster-Shafer evidence theory, and the feasibility and applicability of the model were also verified [22].

Obviously, the above research results are mainly focused on the prediction and prevention of roof water disasters, while there are few studies on the evaluation of the threat degree of water hazard under the superimposed effect of high ground temperature. In addition, the existing methods needing to be improved generally predict the possibility of roof water inrush based on stratum lithology and mining influence, which fails to fully reflect the combined effects of multiple factors such as geology, hydrogeology, geothermal field, and mining failure. Therefore, it is of great significance to

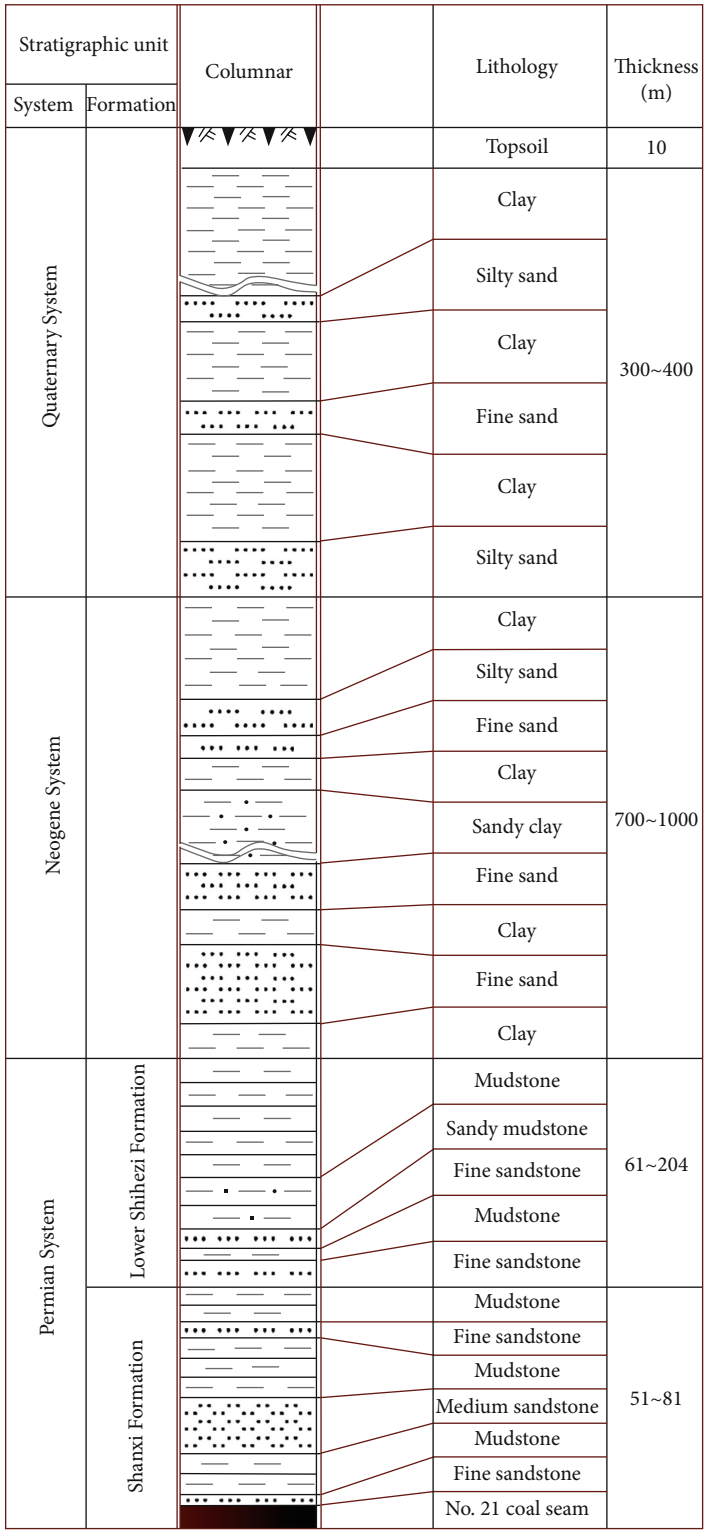

Figure 2: Combined geological column of the stratum.

carry out research on the threat degree of water-heat coupling disaster under deep coal mining conditions.

In this paper, taking the Suiqi coalfield located in the North China coalfield area as the object, based on the collected and measured geothermal well and exploration borehole data, the key evaluation indicators among factors such as the geology, hydrogeology, geothermal field, and mining failure were selected. Then, based on fractal theory, AHP, and fuzzy variable set theory, a mathematical model is constructed, by which the impact degree of the thermal storage

Table 1: The main geological structures in the study area.

Structure	Occurrence factors
Changsi anticline	The axial direction is NW, with a length of approximately 7 km; the two wings are basically symmetrical, and the inclination angles of the two wings are approximately 5°, which is a wide and gentle anticline
Taikang syncline	The axial direction is NW, with a length of approximately 14 km, and the inclination angles of both wings are more than 20°. It is cut by a series of NE trending faults with incomplete morphologies
Liaocheng-Lankao fault	Strike NE, dip NW, dip angle 40~70°, drop greater than 900~4000m
Suixian fault	Strike NE, dip NW, dip angle 60~70°, drop greater than 1000 m, extension length greater than 30 km
Minquan-Yucheng fault	Strike NW, dip NE, dip angle 50~70°, drop greater than 1500 m
Cuiqiao fault	Strike NW, dip SW, dip angle 60~70°, drop 0-800 m, extension length 35 km

aquifer on deep coal mining was quantitatively evaluated. The results can provide technical support for the layout of mining engineering and safety production under the cover of a thermal storage aquifer and can also provide a reference for the identification of roof water and heat disasters in other mining areas in the North China coalfield.

2. Geological and Hydrogeological Characteristics

The Suiqi coalfield (Figure 1), which encompasses an area of approximately 4900 km^2, is located at the junction of Kaifeng City, Shangqiu City, and Zhoukou City in the central part of the North China coalfield area. At a burial depth of 1100~2000 m is the no. 2_1 coal seam, whose average thickness and coal reserves are 5.3 m and 23 billion tons, respectively. With the gradual depletion of coal resources in other areas, to meet the needs of economic and social development, the mining of coal resources in this coalfield will be imperative.

2.1. Geological Characteristics. According to the drilling data, the strata overlying the no. 2_1 coal seam in the coalfield area include the Shanxi Formation (P_1sh) and the Lower Shihezi Formation (P_1x) of the Permian System, the Neogene System (N), and the Quaternary System (Q). The combined geological column of the stratum can be seen in Figure 2.

The geological structure in this area is relatively developed (Figure 1), with Changsi anticline in the north and Taikang syncline in the south. The faults mainly include the Liaocheng-Lankao fault, Suixian fault, Minquan-Yucheng fault, Cuiqiao fault, and other high-angle normal faults. The faults have large drops and extensions, and the occurrence factors are shown in Table 1. These geological structures have destroyed the occurrence of coal seams at different degrees, leading to a lack of coal-bearing strata and changes in the coal thickness.

2.2. Hydrogeological Characteristics. The roof aquifers affect the excavation of the no. 2_1 coal seam of the sandstone fracture aquifer group of the Shanxi Formation and Lower Shihezi Formation and the pore aquifer group of the Neogene period. The water richness of the sandstone fissure aquifer group in the Shanxi Formation and the Xiashihezi Formation is relatively weak, and it has little effect on the mining of the no. 2_1 coal seam in the case of no supply source.

The Neogene aquifer group is mainly composed of a fine sand medium that has good water richness with an average unit water inflow of 0.73 L/(s·m). The aquifer group directly affects the mining of the no. 2_1 coal seam in the hidden outcrop area of the coal seam and indirectly threatens the mining of the no. 2_1 coal seam in other areas through the underlying aquifer group.

The geothermal gradient in this area is between 3.35 and 3.81°C/100 m, with an average value of 3.58°C/100 m. The average temperature of the surrounding rock and groundwater at a depth of 1100 m can reach 54.56°C. The coal mining operations will be affected by abnormally high geothermal disasters.

3. Index Factor Selection and Weight Determination

3.1. Index Factor Selection. The threat degree of the roof thermal storage aquifer during mining in the Suiqi coalfield is mainly controlled by the geological, hydrogeological, and geothermal fields; mining failure; and other factors (as shown in Figure 3).

The geological factors include the overburden structure of the coal seam, the rock thickness, the burial depth of the coal seam roof, and the fault characteristics. The roof of the no. 2_1 coal seam in the coalfield area is an interlayer of brittle sandstone and plastic mudstone. The greater the number of sandstone layers and the greater the thickness of a single layer, the more easily the roof will be damaged under the influence of mining. Therefore, the thickness ratio of the brittle and plastic rock (the ratio of brittle rock thickness to plastic rock thickness) exposed by drilling can be used to characterize the structure and thickness of the coal seam overburden. The deeper the burial depth of the coal seam roof and the thicker the overlying rock layer, the greater the pressure on the roof will be during mining. The more complex the faults of the coal seam roof are, the higher the roof failure height is and the greater the water inrush is. Therefore, the thickness ratio of the brittle and plastic rock, the burial depth of the coal seam roof, and the fault complexity are chosen to reflect the influence of the geological factors in this paper.

The hydrogeological factors include the thickness of the aquifer and the water richness within the height of the "upper three zones" of a roof failure. The greater the thickness and the stronger the water richness, the more water that is provided during the inrush it has and the more harmful it is. The thickness of the aquifer and water richness can be obtained from the drilling and field pumping (injection) water test data. Because the Suiqi coalfield is in the exploration stage, no pumping (injection) water test has been carried

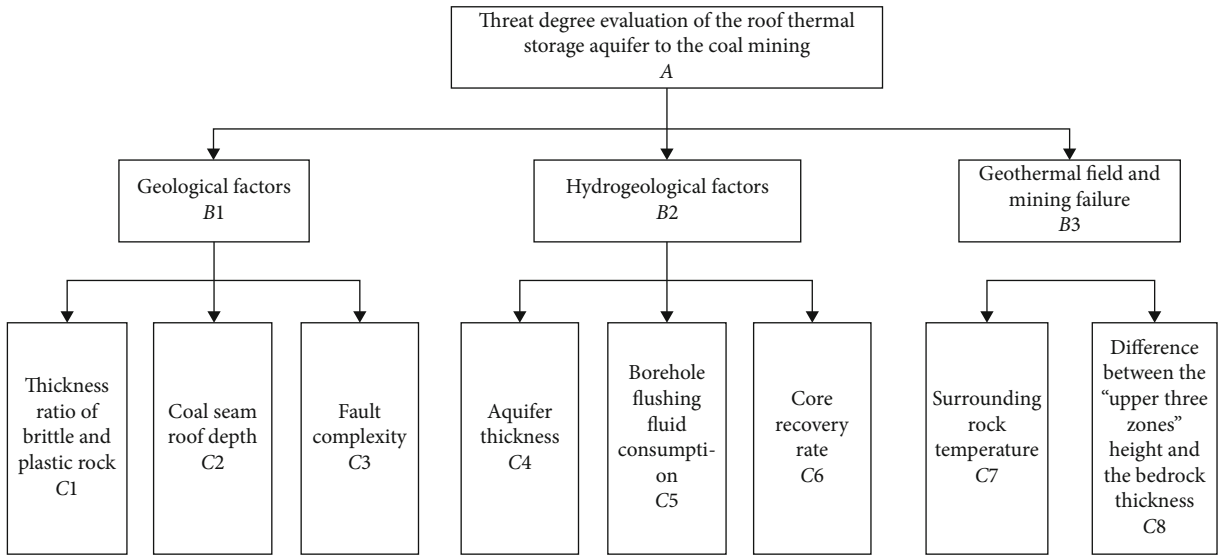

Figure 3: Evaluation index factors of the threat degree during deep coal mining.

Table 2: Judgment matrix $A - B_i$ $(i = 1,2,3)$.

A	B_1	B_2	B_3	$w(A/B_i)$
B_1	1	8/9	7/9	0.2925
B_2	9/8	1	9/7	0.3164
B_3	9/7	9/7	1	0.3911

Note: maximum characteristic value $\lambda_{max} = 3.0016$, CI = 0.0008 < 0.1, and CR = 0.0014 < 0.1.

Table 3: Judgment matrix $B_1 - C_i$ $(i = 1,2,3)$.

B_1	C_1	C_2	C_3	$w(B_1/C_i)$
C_1	1	4/3	1/6	0.1443
C_2	3/4	1	1/5	0.1265
C_3	6	5	1	0.7285

Note: maximum characteristic value $\lambda_{max} = 3.0247$, CI = 0.0124 < 0.1, and CR = 0.0213 < 0.1.

Table 4: Judgment matrix $B_2 - C_i$ $(i = 1,2,3)$.

B_2	C_4	C_5	C_6	$w(B_2/C_i)$
C_4	1	6/5	3/2	0.4000
C_5	5/6	1	5/4	0.3333
C_6	2/3	4/5	1	0.2667

Note: maximum characteristic 5value $\lambda_{max} = 3$, CI = 0 < 0.1, and CR = 0 < 0.1.

Table 5: Judgment matrix $B_3 - C_i$ $(i = 1, 2)$.

B_3	C_7	C_8	$w(B_3/C_i)$
C_7	1	1/3	0.2500
C_8	3	1	0.7500

Note: maximum characteristic value $\lambda_{max} = 2$, CI = 0 < 0.1, and CR = 0 < 0.1.

out at present. In addition, the number of geothermal wells constructed in the area is limited, and it is difficult to obtain the unit water inflow, which characterizes the water richness of the aquifer. In the absence of the unit water inflow, the drill flushing fluid consumption and core recovery rate can be used as a substitute measure [23, 24]. The greater the consumption of flushing fluid during drilling construction, the more developed the pores and cracks in the rock layer are and the stronger the water richness of the aquifer is.

The ground temperature of the Suiqi coalfield is abnormally high. To directly show the threat of the ground temperature field to deep coal seam mining, the surrounding rock temperature at the depth of the coal seam roof is used to indicate its influence. In the Suiqi coalfield, the bedrock composed of sandstone and mudstone is separated between the Neogene thermal reservoir aquifer group and the no. 2_1 coal seam to be mined. The larger the difference between roof failure height and the whole thickness of the bedrock during coal mining, the higher the influence of the Neogene thermal storage aquifer is on the coal seam mining. Therefore, the difference between height of the "upper three zones" and the bedrock thickness is chosen to characterize the impact of a mining failure.

In short, it is reasonable and practical to select the following eight elements as index factors to evaluate the threat degree of the overlying thermal aquifer during coal mining operations: the thickness ratio of brittle and plastic rock, the coal seam roof depth, the fault complexity, the aquifer thickness, the borehole flushing fluid consumption, the core recovery rate, the surrounding rock temperature, and the difference between the height of the "upper three zones" and the bedrock thickness.

According to the water and heat disaster characteristics of a coal seam roof [1], the difference between the height of the "upper three zones" and the bedrock thickness and the complexity of the fault should be the most important levels among the eight index factors; the aquifer thickness, borehole flushing fluid consumption, core recovery rate,

Table 6: Weights of the evaluation index factors.

Index factor	C_1	C_2 (m)	C_3	C_4 (m)	C_5 (m^3/h)	C_6	C_7 (°C)	C_8
Weight	0.0422	0.0370	0.2131	0.1267	0.1055	0.0844	0.0978	0.2933

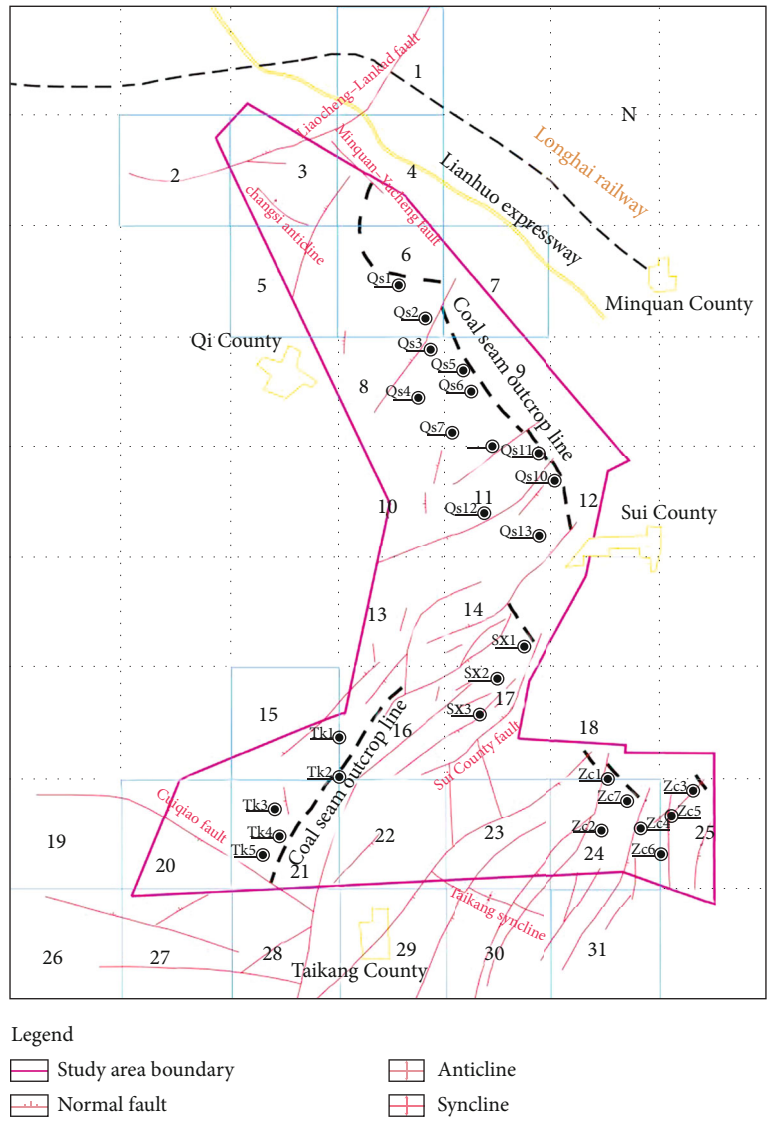

Figure 4: Block number of the study area.

and surrounding rock temperature should be at the second most important influence level, while the coal seam roof depth and thickness ratio of brittle and plastic rock have been reflected in other indexes to some extent, and they should be at the third influence level.

3.2. Index Factor Weight. Referring to the existing results [25], the weights of the eight index factors can be determined by AHP. The judgment matrix of the evaluation system composed of the eight index factors is shown in Tables 2–5.

When the AHP model is used to determine the index factor weights, only when it is established that the consistency index CI < 0.1 and the consistency ratio CR < 0.1 can the judgment matrix and the single order of the factors be logically consistent and can the calculation results be credible. Obviously, the results of all the levels in this paper have passed the consistency test, and the determined index factor weights are credible. The results are shown in Table 6.

4. Quantitative Value of Index Factors Divided

4.1. Fault Complexity. The fractal theory can be used to distinguish the complexity of the faults in the study area [26]. According to a certain scale, the study area is into several square blocks, and the blocks containing faults are counted and numbered. For block i, first divide it according to the

Table 7: Fractal dimension and correlation coefficient of each block.

Block number	Fractal dimension	Correlation coefficient	Block number	Fractal dimension	Correlation coefficient
1	1.2644	0.9893	17	1.5838	0.9981
2	1.0247	0.9665	18	0.9007	0.9836
3	1.1963	0.9879	19	1.3422	0.9730
4	1.0095	0.9648	20	1.4700	0.9820
5	1.0000	1.0000	21	1.3262	0.9705
6	0.7551	0.9884	22	1.3415	0.9903
7	0.6000	0.9000	23	1.5965	0.9823
8	1.1755	0.9854	24	1.4548	0.9841
9	0.9007	0.9836	25	1.4966	0.9853
10	1.1288	0.9968	26	1.3136	0.9862
11	1.4963	0.9721	27	1.5030	0.9809
12	0.8340	0.9902	28	1.2943	0.9927
13	1.2807	0.9661	29	1.4066	0.9713
14	1.5975	0.9823	30	1.3222	0.9950
15	1.0247	0.9665	31	1.0703	0.9749
16	1.8279	0.9941			

Table 8: Fractal dimension values of the faults in the block where the borehole is located.

Borehole number	Fractal dimension	Drilling number	Fractal dimension	Drilling number	Fractal dimension	Drilling number	Fractal dimension
Qs1	0.7551	Qs8	1.1755	Sx2	1.5838	Zc1	1.4548
Qs2	0.7551	Qs9	1.4963	Sx3	1.5838	Zc2	1.4548
Qs3	1.1755	Qs10	1.4963	Tk1	1.0247	Zc3	1.4966
Qs4	1.1755	Qs11	1.4963	Tk2	1.0247	Zc4	1.4548
Qs5	0.9007	Qs12	1.4963	Tk3	1.3262	Zc5	1.4966
Qs6	0.9007	Qs13	1.4963	Tk4	1.3262	Zc6	1.4966
Qs7	0.9007	Sx1	1.5975	Tk5	1.3262	Zc7	1.4548

Table 9: Height calculation formula for the "upper three zones".

Code category	Overburden lithology	Formula 1	Formula 2
Three lower code	Hard lithology	$H_1 = \left(100\sum M/1.2\sum M + 2.0\right) + 18.9$	$H_l = 30\sqrt{\sum M} + 20$
	Medium hard lithology	$H_l = \left(100\sum M/1.6\sum M + 3.6\right) + 15.6$	$H_l = 20\sqrt{\sum M} + 20$
Mining area code	Hard lithology	$H_l = \left(100\sum M/2.4n + 2.1\right) + 21.2$	—
	Medium hard lithology	$H_l = \left(100\sum M/3.3n + 3.8\right) + 15.1$	—

Note: H_l is the height of the upper three zones (m), M is the cumulative mining thickness (m) (when $M < 6$, n takes 1; when $M > 6$, n takes 2), and the bending zone height is taken as 10 m and is directly included in the formula.

magnification of scale $r = 1/2$, and count the number of block segments containing fault trajectories $N(1/2)$; further, divide it according to the scale $r = 1/4, 1/8, 1/16 \cdots$, and count the number of blocks $N(r)$ containing fault trajectories. Then, the fitting straight line equation of lg (r) and lg $N(r)$ can be constructed, and the slope of the line is the fault fractal dimension D of block i. In the same way, the fault fractal dimension of other blocks can be obtained. The larger the fractal dimension D, the more fault traces are contained in the block and the higher the complexity of the fault [27].

The study area is divided into 49 blocks, 31 of which are fault blocks, as shown in Figure 4. According to the above steps, the fractal dimension values of each block can be determined, and the results are shown in Table 7. Obviously, the fault fractal dimension range is 0.7551~1.5838, with an average value of 1.2432. The correlation coefficients of lg (r) and

Table 10: Difference between the height of the "upper three zones" and the bedrock thickness.

Borehole number	Height of the "upper three zones"	Difference between the height of the "upper three zones" and the bedrock thickness	Borehole number	Height of the "upper three zones"	Difference between the height of the "upper three zones" and the bedrock thickness
Qs1	93.27	-39.73	Sx2	122.79	-143.21
Qs2	84.25	-235.14	Sx3	93.47	-156.05
Qs3	139.20	-87.75	Tk1	103.27	-187.55
Qs4	76.06	-263.67	Tk2	49.46	-70.98
Qs5	77.64	15.20	Tk3	97.70	-204.17
Qs6	93.87	-32.37	Tk4	165.11	103.46
Qs7	121.20	-193.92	Tk5	160.77	77.64
Qs8	118.30	21.58	Zc1	91.45	-37.45
Qs9	96.93	-69.22	Zc2	90.87	-175.14
Qs10	48.07	-62.10	Zc3	40.30	-94.38
Qs11	81.42	-73.09	Zc4	111.87	-35.52
Qs12	76.83	-146.91	Zc5	131.20	81.17
Qs13	73.85	-212.14	Zc6	120.76	-33.32
Sx1	97.92	3.81	Zc7	93.18	23.15

lg $N(r)$ of each block are above 0.96, which indicates that the fractal characteristics of the fault distribution in the study area are good under the selected scale. Additionally, the statistical self-similarity of the fractal structure is good, and the fractal dimension value can be used to represent the complexity of the fault.

The 28 geological boreholes belong to different blocks, and the fractal dimension representing the fault complexity is shown in Table 8.

4.2. Difference between the Height of the "Upper Three Zones" and the Bedrock Thickness. After the coal seam is excavated, the roof overburden rock failure is divided into the collapse zone, crack zone, and bending zone (referred to as the "upper three zones"). According to the code for coal pillar reservation and mining under the pressure of buildings, water bodies, railways, and main shafts [28] (referred to as the "three lower code") and the code for hydrogeological engineering geological exploration in a mining area [29] (referred to as the "mining area code"), the height of the "upper three zones" can be calculated by using the empirical formula (Table 9). The maximum value is selected as the basic data for the evaluation in this paper [30] (see Table 10). The bedrock thickness of the coal seam roof can be determined by the drilling exploration results, and the difference between the height of the "upper three zones" and the bedrock thickness is shown in Table 10.

4.3. Index Factor Set. The indexes, such as the thickness ratio of brittle and plastic rock, the aquifer thickness, the borehole flushing fluid consumption, the core recovery rate, the coal seam roof depth, and the surrounding rock temperature within the height of the "upper three zones" of roof failure, can be statistically obtained according to the actual information disclosed by the exploration drilling. For the convenience of evaluation, the reciprocal value of the core recovery rate is taken.

According to the 28 geological boreholes in the Suiqi coalfield, the quantitative values of the 8 index factors used to evaluate the threat degree of the thermal reservoir aquifer are listed in Table 11.

5. Evaluation of the Impact Degree

5.1. Basic Formula. Let a, b, c, d, and k be the points on the fuzzy domain U (see Figure 5), the interval $[a, b]$ belongs to the interval $[c, d]$, and the point k is located at the midpoint of the interval $[a, b]$.

If the intervals $[a, b]$ and $[c, d]$ are denoted by A and B, respectively, u is any sample on U. According to the theory of fuzzy variable sets, the relative difference degree can be calculated as follows.

When u is within interval B and to the left of the k point, then we have the following:

$$\begin{cases} D_A(u) = \left(\dfrac{u-a}{k-a}\right)^{\beta}, & u \in [a, k], \\ D_A(u) = -\left(\dfrac{u-a}{c-a}\right)^{\beta}, & u \in [c, a]. \end{cases} \tag{1}$$

When u is within interval B and to the right of the k point, then we have the following:

$$\begin{cases} D_A(u) = \left(\dfrac{u-b}{k-b}\right)^{\beta}, & u \in [k, b], \\ D_A(u) = -\left(\dfrac{u-b}{d-b}\right)^{\beta}, & u \in [b, d]. \end{cases} \tag{2}$$

Table 11: Evaluation index value of the threat degree of the thermal storage aquifer.

Borehole number	Index factor							
	C_1	C_2	C_3	C_4	C_5	C_6	C_7	C_8
Qs1	0.8224	1470.12	0.7551	42.09	1.9383	1.3966	56.18	-39.73
Qs2	1.0064	1561.16	0.7551	42.26	0.0416	1.2005	58.68	-235.14
Qs3	0.9559	1468.39	1.1755	62.57	0.2300	1.2092	56.13	-87.75
Qs4	1.0053	1691.00	1.1755	38.65	0.0399	1.1338	62.25	-263.67
Qs5	1.5949	1334.97	0.9007	47.72	3.1990	1.7212	52.46	15.20
Qs6	1.8727	1325.76	0.9007	32.11	0.0506	1.1038	52.21	-32.37
Qs7	0.8099	1526.42	0.9007	48.42	0.0890	1.1792	57.73	-193.92
Qs8	1.7077	1264.02	1.1755	59.43	2.9629	1.5949	50.51	21.58
Qs9	0.7841	1352.94	1.4963	42.60	1.8820	1.2690	52.96	-69.22
Qs10	1.5810	1204.30	1.4963	27.51	0.7990	1.3986	48.87	-62.10
Qs11	1.7095	1364.02	1.4963	51.37	0.2496	1.0834	53.26	-73.09
Qs12	0.1789	1521.00	1.4963	11.66	0.9416	1.1601	57.58	-146.91
Qs13	0.3719	1493.27	1.4963	20.14	0.1394	1.1403	56.81	-212.14
Sx1	0.2864	1261.70	1.5975	17.85	2.1440	1.4327	47.59	3.81
Sx2	0.9584	1393.03	1.5838	39.16	1.6810	1.4085	50.90	-143.21
Sx3	0.6118	1450.83	1.5838	30.39	0.0402	1.3850	52.36	-156.05
Tk1	0.4415	1570.14	1.0247	29.82	0.1799	1.1173	64.51	-187.55
Tk2	0.4131	1376.04	1.0247	14.46	0.0402	1.1390	58.47	-70.98
Tk3	0.5381	1565.08	1.3262	24.13	0.0460	1.0905	64.35	-204.17
Tk4	1.1794	1357.85	1.3262	29.80	2.9678	1.7301	57.91	103.46
Tk5	0.8309	1388.23	1.3262	45.42	2.8799	1.5748	58.85	77.64
Zc1	0.4629	1277.50	1.4548	28.88	2.3816	1.8315	47.99	-37.45
Zc2	0.9228	1460.61	1.4548	38.60	2.2623	1.6000	52.60	-175.14
Zc3	0.2077	1221.04	1.4966	4.31	0.3990	1.1274	46.57	-94.38
Zc4	1.5399	1339.83	1.4548	40.25	2.0805	1.9157	49.56	-35.52
Zc5	1.4500	1202.78	1.4966	37.84	0.1294	1.1806	46.11	81.17
Zc6	2.2950	1318.17	1.4966	50.32	0.1218	1.2579	49.01	-33.32
Zc7	0.4280	1270.66	1.4548	39.88	2.6783	1.6026	47.82	23.15
Mean value ρ	0.9631	1393.9593	1.2972	35.6300	1.1641	1.3566	53.94	-79.56
Standard deviation σ	0.5547	123.3001	0.2623	13.7339	1.1509	0.2446	5.17	98.33

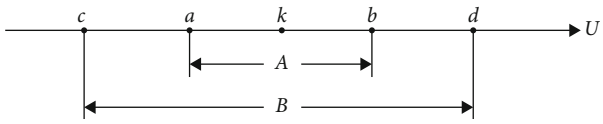

Figure 5: Schematic diagram of the location of the intervals $[a, b]$ and $[c, d]$.

When u does not belong to interval B, then we have the following:

$$D_A(u) = -1, \tag{3}$$

where β is an index greater than 0, and usually $\beta = 1$.

After using formulas (1)–(3) to obtain the relative difference degree $D_A(u)$, the following formula can be used to calculate the relative membership degree $\mu_A(u)$:

$$\mu_A(u) = \frac{1 + D_A(u)}{2}. \tag{4}$$

If there are n interval levels on the domain U and the sample u is composed of m index factors, the comprehensive relative membership degree of the sample u belonging to level h can be calculated as follows:

$$\varphi_h(u) = \left\{ 1 + \left[\frac{\sum_{i=1}^{m} [w_i (1 - \mu_h(\mu_i))]^p}{\sum_{i=1}^{m} [w_i \mu_h(\mu_i)]^p} \right]^{\alpha/p} \right\}^{-1}, \tag{5}$$

where $\mu_h(u_i)$ is the relative membership of the index factor; w_i is the weight of the index factor; $i = 1, 2, \cdots, m$; $h = 1, 2, \cdots, n$; α is the optimization criterion parameter ($\alpha = 1$ or $\alpha = 2$); and p is the distance parameter ($p = 1$ is the Hamming distance and $p = 2$ is the Euclidean distance).

Table 12: Classification of the threat degree of the thermal reservoir aquifer.

Threat level	Safe (I)	Low threat (II)	Medium threat (III)	Relatively high threat (IV)	High threat (V)
Level characteristic value	$H \le 2.0$	$2.0 < H \le 2.5$	$2.5 < H \le 3.0$	$3.0 < H \le 3.5$	$H > 3.5$

Table 13: Calculation formula for the $[a, b]$ and $[c, d]$ assignment.

Threat level	Safe (I)	Low threat (II)	Medium threat (III)	Relatively high threat (IV)	High threat (V)
$[a, b]$	$[\rho - 1.25\sigma, \rho - 0.75\sigma]$	$[\rho - 0.75\sigma, \rho - 0.25\sigma]$	$[\rho - 0.25\sigma, \rho + 0.25\sigma]$	$[\rho + 0.25\sigma, \rho + 0.75\sigma]$	$[\rho + 0.75\sigma, \rho + 1.25\sigma]$
$[c, d]$	$[\rho - 1.5\sigma, \rho - 0.5\sigma]$	$[\rho - \sigma, \mu]$	$[\rho - 0.5\sigma, \rho + 0.5\sigma]$	$[\rho, \rho + \sigma]$	$[\rho + 0.5\sigma, \rho + 1.5\sigma]$
k	$\rho - \sigma$	$\rho - 0.5\sigma$	ρ	$\rho + 0.5\sigma$	$\rho + \sigma$

Note: ρ and σ are the mean and standard deviation of the index factor, respectively; when a or c is less than 0, its value is 0.

Table 14: Composition of matrix AB.

Index factor	Threat level				
	Safe (I)	Low threat (II)	Medium threat (III)	Relatively high threat (IV)	High threat (V)
C_1	[0.27, 0.55]	[0.55, 0.82]	[0.82, 1.10]	[1.10, 1.38]	[1.38, 1.66]
C_2	[1239.83, 1301.48]	[1301.48, 1363.13]	[1363.13, 1424.78]	[1424.78, 1486.43]	[1486.43, 1548.08]
C_3	[0.97, 1.10]	[1.10, 1.23]	[1.23, 1.36]	[1.36, 1.49]	[1.49, 1.63]
C_4	[18.46, 25.33]	[25.33, 32.20]	[32.20, 39.06]	[39.06, 45.93]	[45.93, 52.80]
C_5	[0, 0.30]	[0.3, 0.88]	[0.88, 1.45]	[1.45, 2.03]	[2.03, 2.60]
C_6	[1.05, 1.17]	[1.17, 1.30]	[1.30, 1.42]	[1.42, 1.54]	[1.54, 1.66]
C_7	[47.48, 50.06]	[50.06, 52.65]	[52.65, 55.23]	[55.23, 57.82]	[57.82, 60.40]
C_8	[-202.48, -153.31]	[-153.31, -104.15]	[-104.15, -54.98]	[-54.98, -5.81]	[-5.81, 43.35]

Table 15: Composition of matrix CD.

Index factor	Threat level				
	Safe (I)	Low threat (II)	Medium threat (III)	Relatively high threat (IV)	High threat (V)
C_1	[0.13, 0.69]	[0.41, 0.96]	[0.69, 1.24]	[0.96, 1.52]	[1.24, 1.80]
C_2	[1209.01, 1332.31]	[1270.66, 1393.96]	[1332.31, 1455.61]	[1393.96, 1517.26]	[1455.61, 1578.91]
C_3	[0.90, 1.17]	[1.03, 1.30]	[1.17, 1.43]	[1.30, 1.56]	[1.43, 1.69]
C_4	[15.03, 28.76]	[21.90, 35.63]	[28.76, 42.50]	[35.63, 49.36]	[42.50, 56.23]
C_5	[0, 0.59]	[0.01, 1.16]	[0.59, 1.74]	[1.16, 2.32]	[1.74, 2.89]
C_6	[0.99, 1.23]	[1.11, 1.36]	[1.23, 1.48]	[1.36, 1.60]	[1.48, 1.72]
C_7	[46.19, 51.36]	[48.77, 53.94]	[51.36, 56.52]	[53.94, 59.11]	[56.52, 61.69]
C_8	[-227.07, -128.73]	[-177.90, -79.56]	[-128.73, -30.4]	[-79.56, 18.77]	[-30.4, 67.94]

The calculation formula of the level characteristic value of sample u is as follows:

$$H(u) = \sum_{h=1}^{n} \frac{\varphi_h(u)}{\sum_{h=1}^{n} \varphi_h(u)} h. \tag{6}$$

According to the level characteristic value $H(u)$, the level of the sample u can be judged.

5.2. Level Matrix Construction. In view of the fact that the overlying thermal storage aquifer in the study area has good water richness and is affected by a high ground temperature, referring to the existing research results [31], the threat degree of the overlying thermal storage aquifer of the coal seam is divided into five levels, i.e., safe, low threat, medium threat, relatively high threat, and high threat, which are expressed as I, II, III, IV, and V, respectively. The corresponding level characteristic values are shown in Table 12.

For a certain evaluation index factor, the intervals $[a, b]$ and $[c, d]$ corresponding to the five levels can be determined according to the mean-standard deviation method [32]. k is the average value of a and b, and the specific calculation formula is shown in Table 13.

Table 16: Composition of matrix K.

Index factor	Threat level				
	Safe (I)	Low threat (II)	Medium threat (III)	Relatively high threat (IV)	High threat (V)
C_1	0.4084	0.6858	0.9631	1.2405	1.5178
C_2	1270.66	1332.31	1393.96	1455.61	1517.26
C_3	1.0349	1.1661	1.2972	1.4284	1.5595
C_4	21.8961	28.7631	35.6300	42.4970	49.3639
C_5	0.0132	0.5887	1.1641	1.7396	2.3150
C_6	1.1120	1.2343	1.3566	1.4789	1.6012
C_7	48.7721	51.3561	53.9400	56.5240	59.1079
C_8	-177.8983	-128.7312	-79.5640	-30.3969	18.7703

Table 17: Relative difference matrix of borehole Qs1.

Index factor	Threat level				
	Safe (I)	Low threat (II)	Medium threat (III)	Relatively high threat (IV)	High threat (V)
C_1	-1	-0.0171	0.0171	-1	-1
C_2	-1	-1	-1	0.5291	-0.5292
C_3	-1	-1	-1	-1	-1
C_4	-1	-1	-0.8808	0.8821	-1
C_5	-1	-1	-1	0.3162	-0.3162
C_6	-1	-1	0.39	-0.39	-1
C_7	-1	-1	-0.6218	0.6242	-1
C_8	-1	-0.5081	-0.6204	0.6203	-1

Table 18: Relative membership matrix of borehole Qs1.

Index factor	Threat level				
	Safe (I)	Low threat (II)	Medium threat (III)	Relatively high threat (IV)	High threat (V)
C_1	0	0.4914	0.5086	0	0
C_2	0	0	0	0.7646	0.2354
C_3	0	0	0	0	0
C_4	0	0	0.0596	0.9410	0
C_5	0	0	0	0.6581	0.3419
C_6	0	0	0.6950	0.3050	0
C_7	0	0	0.1891	0.8121	0
C_8	0	0	0.1899	0.8101	0

According to the assignment criteria in Table 13, the AB, CD, and K matrices are composed of the index factors and threat levels can be obtained, as shown in Tables 14–16.

Table 19: Comprehensive membership matrix of borehole Qs1.

Parameter assignment	Threat level				
	Safe (I)	Low threat (II)	Medium threat (III)	Relatively high threat (IV)	High threat (V)
$\alpha = 1, p = 1$	0	0.0207	0.1618	0.5597	0.0448
$\alpha = 1, p = 2$	0	0.0470	0.1892	0.5505	0.0822
$\alpha = 2, p = 1$	0	0.0004	0.0359	0.6177	0.0022
$\alpha = 2, p = 2$	0	0.0024	0.0516	0.6000	0.0080

Table 20: Level characteristic values of borehole Qs1.

Parameter assignment	Threat level					Sum
	Safe (I)	Low threat (II)	Medium threat (III)	Relatively high threat (IV)	High threat (V)	
$\alpha = 1, p = 1$	0	0.0527	0.6169	2.8446	0.2845	3.7987
$\alpha = 1, p = 2$	0	0.1081	0.6531	2.5344	0.4731	3.7685
$\alpha = 2, p = 1$	0	0.0014	0.1643	3.7649	0.0167	3.9472
$\alpha = 2, p = 2$	0	0.0073	0.2339	3.6254	0.0601	3.9267
Mean value	0	0.0424	0.4170	3.1933	0.2074	3.8603

5.3. Evaluation Results. For the borehole Qs1, the relative difference degree and relative membership degree (as shown in Tables 17 and 18) can be obtained by using formulas (1)–(6); then, the comprehensive membership degree and level characteristic values (as shown in Tables 19 and 20) under different parameters α and p can be further calculated. The calculation results show that the average level characteristic value of borehole Qs1 is 3.8603, which belongs to a high-threat area according to the classification standard in Table 12. According to the calculation steps of borehole Qs1, the level characteristic values of 28 boreholes can be given in turn, as shown in Table 21.

It can be seen from Table 21 that the proportion of the 28 boreholes that are in the high threat and relatively high threat levels is 57.14%, 32.14% of the boreholes are in the medium threat and low threat levels, and 10.71% of the boreholes are in the safe level.

Contour maps can be drawn based on the average level characteristic values of the 28 boreholes, and the threat degree division of the overlying thermal storage aquifer under the condition of coal mining can be delineated according to the criteria in Table 13, as shown in Figure 6.

The overall threat degree of the roof thermal storage aquifer is as follows: the threat degree in the western portion of the study area is less than that in the eastern portion, and the threat degree increases as the hidden outcrop line of the coal seam is approached. Due to the influences of multiple factors, the average level characteristic value H of the areas near the boreholes Qs1,Qs5, Qs8, Sx1, Tk5, Zc4, and Zc7,

Table 21: Borehole level characteristic value and threat degree level.

Borehole number	Level characteristic value				Mean value	Threat degree level
	$\alpha = 1$, $p = 1$	$\alpha = 1$, $p = 2$	$\alpha = 2$, $p = 1$	$\alpha = 2$, $p = 2$		
Qs1	3.7987	3.7685	3.9472	3.9267	3.8603	V
Qs2	3.1859	3.1691	3.4444	3.4207	3.3050	IV
Qs3	2.5265	2.5628	2.4522	2.5588	2.5250	III
Qs4	2.2011	2.2613	2.0194	2.0668	2.1372	II
Qs5	4.2872	4.1676	4.8764	4.8075	4.5347	V
Qs6	1.8210	1.8441	1.6587	1.6617	1.7464	I
Qs7	2.5865	2.6138	1.8951	1.8889	2.2461	II
Qs8	3.5078	3.4391	4.0806	3.9407	3.7421	V
Qs9	3.4943	3.4589	3.5209	3.5204	3.4986	IV
Qs10	3.1276	3.1309	3.2121	3.2368	3.1768	IV
Qs11	3.2272	3.2326	3.3266	3.3260	3.2781	IV
Qs12	2.9278	2.8802	2.7781	2.6720	2.8145	III
Qs13	2.5854	2.9463	1.7968	2.5684	2.4742	II
Sx1	3.8993	3.9521	4.5876	4.6299	4.2672	V
Sx2	3.0592	3.0541	2.9384	3.0072	3.0147	IV
Sx3	2.5640	2.7300	2.1946	2.5243	2.5032	III
Tk1	1.2672	1.3886	1.0412	1.0935	1.1976	I
Tk2	2.7366	2.9585	2.6189	2.9054	2.8048	III
Tk3	1.8434	2.1897	1.2607	1.7741	1.7670	I
Tk4	3.1855	3.1930	3.0486	2.9762	3.1008	IV
Tk5	3.9012	3.7841	3.9331	3.7070	3.8313	V
Zc1	3.3253	3.3231	3.6613	3.6741	3.4959	IV
Zc2	2.9098	2.7651	2.6888	2.2687	2.6581	III
Zc3	2.7722	3.1029	2.5133	3.2040	2.8981	III
Zc4	3.7228	3.5441	3.9969	3.9215	3.7963	V
Zc5	3.1836	3.1898	3.3773	3.4149	3.2914	IV
Zc6	3.3586	3.4039	3.3745	3.8063	3.4858	IV
Zc7	3.8714	3.8507	4.4635	4.4201	4.1514	V

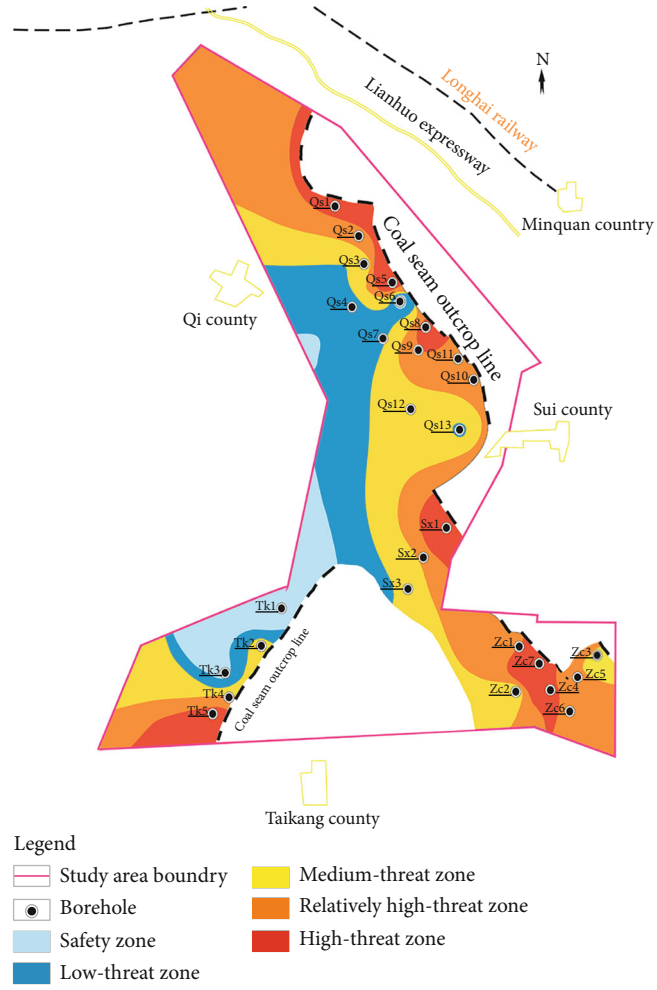

Figure 6: Threat degree division of the coal seam roof.

which are close to the hidden outcrop line of the coal seam, is greater than 3.5, which are the high-threat areas caused by the roof thermal storage aquifer.

According to the statistical results in Figure 6, it can be seen that the high-threat zone of the roof thermal storage aquifer accounts for 10.21% of the study area, the relatively high-threat zone accounts for 33.85%, the medium-threat zone accounts for 27.76%, the low-threat zone accounts for 19.76%, and the safe zone accounts for 8.42%. Obviously, the proportion of the area above the medium-threat zone is 71.82%, and the possibility of a roof water and heat disaster accident occurring under coal mining conditions is greater.

5.4. Verification of Evaluation Results. According to the "upper three zones" theory of a coal seam roof, when the calculated height of the "upper three zones" is greater than the thickness of the bedrock, the roof failure zone of the coal mining operation will reach the overlying Neogene thermal storage aquifer with strong water richness and good permeability, which will greatly increase the risk of a roof disaster. Therefore, the difference between the thickness of the coal seam roof bedrock and the height of the "upper three zones" (referred to as "difference") is a common index and a traditional method to evaluate the roof threat level at present. The smaller the "difference" is, the greater the roof threat level is. The areas where the "difference" is negative belong to the high-threat areas of the roof.

The "difference" contour of the Suiqi coalfield is shown in Figure 7. Obviously, the "difference" in the west is larger than that in the east during the mining of the no. 2_1 coal seam, which indicates that the roof disaster threat is greater as the hidden outcrop line of the coal seam is approached. In addition, the high-threat area of the roof in Figure 7 is located in the high-threat area and relatively high-threat area in Figure 6, which shows that the evaluation results of the "difference" method and the method adopted in this paper are basically the same. However, the fuzzy variable set method adopted in this paper considers more influencing factors and can obtain more precise evaluation results.

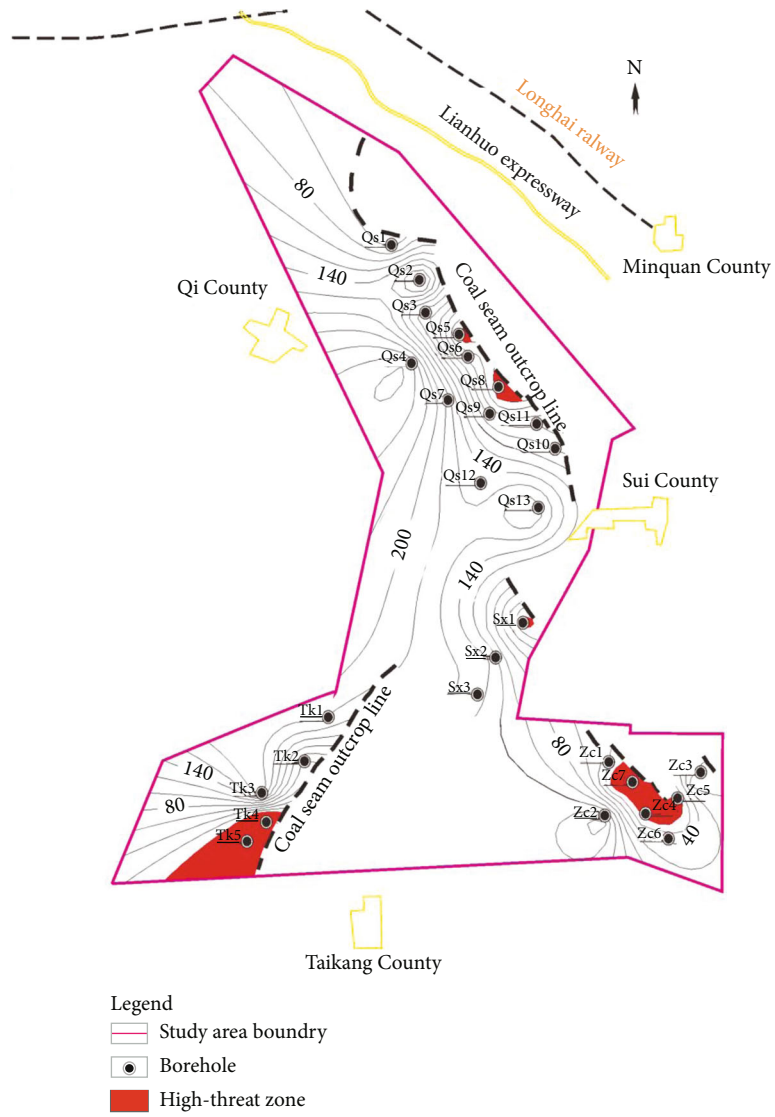

Figure 7: Difference contour diagrams between the thickness of the roof bedrock and the height of the "upper three zones."

6. Conclusions

(1) Based on the analysis of multiple factors affecting coal mining, eight factors are selected as the index factors for threat assessment, including the thickness ratio of brittle and plastic rock, the coal seam roof depth, the fault complexity, the aquifer thickness, the borehole flushing fluid consumption, the core recovery rate, the surrounding rock temperature, and the difference between the height of the "upper three zones" and the bedrock thickness, which provide a guarantee for the comprehensive and accurate identification of water and heat disasters of coal seam roofs

(2) The mathematical model of the threat degree evaluation is established by coupling the AHP and the fuzzy variable set theory. Based on the weights and quantitative values of the eight index factors, the threat degree of the thermal storage aquifer to the deep coal mining operation was identified and the threat degree was divided, which lays the foundation for the prevention and control of water and heat disasters of the overlying strata and safe mining

(3) The quantitative evaluation of the threat degree of the thermal storage aquifer shows that the risk in the western region is less than that in the eastern region, and the closer it is to the outcrop line of the coal seam, the greater the risk; in the areas near the boreholes Qs1,Qs5, Qs8, Sx1, Tk5, Zc4, and Zc7, which are close to the hidden outcrop line of the coal seam, the classification characteristic values of the threat degree are greater than 3.5, which belong to high-threat areas caused by the roof thermal storage aquifer. In these areas, roof water and heat disasters are prone to occur during coal mining

(4) According to the threat degree of the thermal storage aquifer of the coal seam roof, comparing the

evaluation results of the traditional "upper three zones" theory (taking the difference between the thickness of the bedrock and the height of the "upper three zones" as parameters) with modern mathematical methods (coupling AHP and variable fuzzy set theory), it can be obtained that the evaluation results of the two methods are basically the same, but the evaluation results of the latter are more precise

(5) For the entire study area, the high-threat zone accounts for 10.21%, the relatively high-threat zone accounts for 33.85%, the medium-threat zone accounts for 27.76%, the low-threat zone accounts for 19.76%, and the safe zone accounts for 8.42%. The area above the medium-threat zone accounts for 71.82%, which includes a greater possibility of the roof water and a heat disaster occurring during mining of the no. 2_1 coal seam

Data Availability

All data used to support the findings of this study are available from the corresponding author upon request.

Conflicts of Interest

The authors declare that they have no conflicts of interest.

Acknowledgments

This work was supported by the National Natural Science Foundation of China (Grant nos. 41672240 and 41972254), the Innovation Scientists and Technicians Troop Construction Projects of Henan Province (Grant no. CXTD2016053), and the Fundamental Research Funds for Henan Polytechnic University (NSFRF200103).

References

[1] M. G. Qian and T. C. Liu, *Mine Pressure and Its Control*, Coal Industry Press, Beijing, 1984.

[2] Q. D. Qu, J. L. Xu, R. L. Wu, W. Qin, and G. Z. Hu, "Three–zone characterisation of coupled strata and gas behaviour in multi-seam mining," *International Journal of Rock Mechanics and Mining Sciences*, vol. 78, pp. 91–98, 2015.

[3] Z. P. Meng, X. C. Shi, and G. Q. Li, "Deformation, failure and permeability of coal-bearing strata during longwall mining," *Engineering Geology*, vol. 208, pp. 69–80, 2016.

[4] L. S. Jiang, Q. S. Wu, Q. L. Wu et al., "Fracture failure analysis of hard and thick key layer and its dynamic response characteristics," *Engineering Failure Analysis*, vol. 98, pp. 118–130, 2019.

[5] L. J. Zhai and C. X. Li, "Application of tri figure–double prediction methods in water disaster prevention and treatment evaluation of Pingshuo no. 3 mine shaft top roof," *Procedia Earth and Planetary Science*, vol. 3, pp. 470–476, 2011.

[6] A. J. Das, P. K. Mandal, S. P. Sahu, A. Kushwaha, R. Bhattacharjee, and S. Tewari, "Evaluation of the effect of fault on the stability of underground workings of coal mine through DEM and statistical analysis," *Journal of the Geological Society of India*, vol. 92, no. 6, pp. 732–742, 2018.

[7] Y. X. Zhang, S. H. Tu, Q. S. Bai, and J. J. Li, "Overburden fracture evolution laws and water-controlling technologies in mining very thick coal seam under water-rich roof," *International Journal of Mining Science and Technology*, vol. 23, no. 5, pp. 693–700, 2013.

[8] S. F. Wang, X. B. Li, and S. Y. Wang, "Separation and fracturing in overlying strata disturbed by longwall mining in a mineral deposit seam," *Engineering Geology*, vol. 226, pp. 257–266, 2017.

[9] K. F. Fan, W. P. Li, Q. Q. Wang et al., "Formation mechanism and prediction method of water inrush from separated layers within coal seam mining: a case study in the Shilawusu mining area, China," *Engineering Failure Analysis*, vol. 103, pp. 158–172, 2019.

[10] C. J. Booth and E. P. Breuer, "Using MODFLOW with TMR to model hydrologic effects and recovery in the shallow aquifer system above longwall coal mining," in *10th International-Mine-Water-Association Congress on Mine Water and the Environment*, pp. 11–14, Karlovy Vary, Czech Republic, 2008.

[11] Q. Wu, Y. Z. Liu, L. H. Luo, S. Q. Liu, W. J. Sun, and Y. F. Zeng, "Quantitative evaluation and prediction of water inrush vulnerability from aquifers overlying coal seams in Donghuantuo coal mine, China," *Environmental Earth Sciences*, vol. 74, no. 2, pp. 1429–1437, 2015.

[12] Y. D. Zhou, Z. X. Li, C. P. Li, and Z. G. Cao, "Design and realization of mine water-inrush visualization simulation system," *Advanced Materials Research*, vol. 383-390, pp. 6632–6640, 2011.

[13] H. W. Zhang, Z. J. Zhu, L. J. Huo, Y. Chen, and B. J. Huo, "Overburden failure height of superhigh seam by fully mechanized caving method," *Journal of China Coal Society*, vol. 39, no. 5, pp. 816–821, 2014.

[14] Y. Yang and Q. F. Sun, "Two–band height observation of Gaotouyao coal mine 2-3 coal seam and safety mining under water," *Safety in Coal Mines*, vol. 46, no. 12, pp. 73–76, 2015.

[15] B. H. Yao, H. B. Bai, and B. Y. Zhang, "Numerical simulation on the risk of roof water inrush in Wuyang coal mine," *International Journal of Mining Science and Technology*, vol. 22, no. 2, pp. 273–277, 2012.

[16] J. Zhang and T. Yang, "Study of a roof water inrush prediction model in shallow seam mining based on an analytic hierarchy process using a grey relational analysis method," *Arabian Journal of Geosciences*, vol. 11, no. 7, 2018.

[17] Q. Wu, Y. Z. Liu, W. F. Zhou et al., "Evaluation of water inrush vulnerability from aquifers overlying coal seams in the Menkeqing coal mine, China," *Mine Water and the Environment*, vol. 34, no. 3, pp. 258–269, 2015.

[18] Y. F. Zeng, Q. Wu, S. Q. Liu, Y. L. Zhai, H. Q. Lian, and W. Zhang, "Evaluation of a coal seam roof water inrush: case study in the Wangjialing coal mine, China," *Mine Water and the Environment*, vol. 37, no. 1, pp. 174–184, 2018.

[19] X. B. Ren and R. F. Wu, "A modified three graphics–two predictions method based on hydraulic pressure of aquifers above coal seam roof," *Coal Engineering*, vol. 48, no. 11, pp. 131–133, 2016.

[20] M. Rezaei, "Development of an intelligent model to estimate the height of caving–fracturing zone over the longwall gobs," *Neural Computing and Applications*, vol. 30, no. 7, pp. 2145–2158, 2018.

[21] H. J. Guo, M. Ji, K. Chen, Z. L. Zhang, Y. D. Zhang, and M. L. Zhang, "The feasibility of mining under a water body based on a fuzzy neural network," *Mine Water and the Environment*, vol. 37, no. 4, pp. 703–712, 2018.

[22] Z. Ruan, C. Li, A. Wu, and Y. Wang, "A new risk assessment model for underground mine water inrush based on AHP and D-S evidence theory," *Mine Water and the Environment*, vol. 38, no. 3, pp. 488–496, 2019.

[23] Z. L. Huo, "Field research on developing height of overlying strata overlying strata of thick layer fully-mechanized mining working face in Sihe mine," *Morden Mining*, vol. 12, pp. 7–11, 2012.

[24] G. Fang, "Risk evaluation of roof water inflow (inrush) and prevention and control measures in early mining areas of Balasu coal mine," *Safety in Coal Mines*, vol. 49, no. 12, pp. 189–193, 2018.

[25] F. Feng and L. He, "CBM block capacity potential partitioning based on AHP–a case study of coal no. 3 in Shizhuang north block, Shanxi," *Coal Geology of China*, vol. 30, no. 6, pp. 51–54, 2018.

[26] B. B. Mandelbrot, *The Fractal Geometry of Nature (Updated and Augmented Edition)*, W. H. Freeman and Company, New York, 1983.

[27] R. Z. Li, Q. Wang, X. Y. Wang, X. Liu, J. Li, and Y. Zhang, "Relationship analysis of the degree of fault complexity and the water irruption rate, based on fractal theory," *Mine Water and the Environment*, vol. 36, no. 1, pp. 18–23, 2017.

[28] State Administration of Safety Supervision, *Coal Pillar Reservation and Mining under Pressure of Buildings, Water bodies, Railways and Main shafts*, China Standard Press, Beijing, 2017.

[29] State Bureau of Technical Supervision, "Hydrogeological engineering geological exploration in mining area," China Standard Press, Beijing, 1991.

[30] Y. C. Xu, J. C. Li, S. Q. Liu, and L. Zhou, "Calculation formula of two-zone height of overlying strata and its adaptability analysis," *Coal mining Technology*, vol. 16, no. 2, pp. 4–7, 2011.

[31] X. Y. Wang, Y. Zou, Q. Wang et al., "Quantitative evaluation of karst developmental differences based on improved analytic hierarchy process and multidimensional extension matter element model," *Geofluids*, vol. 2019, Article ID 5093237, 12 pages, 2019.

[32] S. Chen and T. Wang, "Comparison analyses of equal interval method and mean-standard deviation method used to delimitate urban heat island," *Geo-information Science*, vol. 11, no. 2, pp. 145–150, 2009.